Appendix A. Supplementary Tables

Supplementary Table A.1: REDBACK input parameters for various relative plate-motion datasets[a]

Plate pair	EU-NA	NB-NA	SO-AN	PA-AN	NB-AN	NB-SA
ensemble_size	2e7	2e7	2e7	2e7	2e7	2e7
burn_in	2e5	2e5	2e5	2e5	2e5	2e5
max_partitions	20	20	34	34	34	34
time_sigma	1.0	1.0	1.0	0.1	0.8	1.0
lon_sigma	1.0	1.0	0.5	0.7	1.5	1.0
lat_sigma	1.0	0.3	1.0	1.0	2.5	1.0
ang_sigma	0.07	0.1	0.01	0.1	0.05	0.02
lon_sigma_bd	1.0	1.0	0.5	0.7	1.5	1.0
lat_sigma_bd	1.0	0.3	1.0	1.0	2.5	1.0
ang_sigma_bd	0.07	0.1	0.01	0.1	0.05	0.02
hp_lon_min	0.1	0.1	0.1	0.1	0.1	0.1
hp_lon_max	15.0	30.0	15.0	20.0	10.0	10.0
hp_lon_sigma	1.0	1.0	0.5	0.5	0.5	0.05
hp_lat_min	0.1	0.1	0.1	0.1	0.1	0.1
hp_lat_max	30.0	20.0	10.0	20.0	10.0	20.0
hp_lat_sigma	1.5	0.5	1.5	0.1	0.12	0.5
hp_ang_min	0.1	0.1	0.1	0.1	0.1	0.1
hp_ang_max	15.0	20.0	10.0	20.0	10.0	10.0
hp_ang_sigma	0.1	0.1	0.05	0.1	0.05	0.1

[a]Referenced best-fitting finite rotation datasets are obtained from the following authors: South America relative to Nubia (SA-NB) from DeMets and Merkouriev (2019), Antarctica-Nubia (AN-NB) and Somalia-Antarctica (SO-AN) from DeMets et al. (2021), the North America-Nubia (NA-NB) and North America-Eurasia (NA-EU) systems from DeMets et al. (2015), and those of Pacific-Antarctica (PA-AN) from Croon et al. (2008).

Supplementary Table A.2: Geomagnetic Polarity Time Scale GTS20 from Ogg (2020)

Magnetic reversal	Age (Ma)	Magnetic reversal	Age (Ma)
1no	0.773	5An.2nm	12.373
2ny	1.775	5An.2o	12.474
2nm	1.8545	5AAnm	13.1075
2An.1y	2.595	5ACy	13.739
2An.3o	3.596	5ADnm	14.386
3n.1y	4.187	5ADo	14.609
3n.1nm	4.2435	5Bn.2nm	15.096
3n.4nm	5.1160	5Cn.1y	15.974
3n.4o	5.235	5Cn.1nm	16.121
3An.1y	6.023	5Cn.3nm	16.632
3An.2o	6.727	5Dy	17.235
4n.1y	7.537	5Dnm	17.384
4n.2nm	7.913	5Ey	18.007
4n.2o	8.125	6ny	18.636
4Anm	8.938	6no	19.535
4Ao	9.105	6An.2nm	20.6065
5n.1y	9.786	6An.2o	20.765
5n.2o	11.056		

Astronomically-tuned timescale for the relevant reversals of this work.

Supplementary Table A.3: South America-Nubia relative motion Euler vectors and covariances

t_{final}	$t_{initial}$	Lat.	Lon.	ω	Covariance elements [10^{-8} rad^2 Myr^{-2}]					
[Myr]	[Myr]	[°N]	[°E]	[°Myr^{-1}]	c_{xx}	c_{xy}	c_{xz}	c_{yy}	c_{yz}	c_{zz}
0.773	1.775	-61.48	139.99	0.298	1.21	-0.66	0.90	0.73	-0.84	3.27
1.775	2.595	-61.52	139.85	0.298	1.12	-0.53	0.53	0.62	-0.56	2.46
2.595	3.596	-61.41	139.95	0.298	0.99	-0.48	0.49	0.55	-0.51	2.20
3.596	4.187	-61.26	140.10	0.298	0.94	-0.49	0.55	0.58	-0.53	2.25
4.187	5.235	-61.11	140.26	0.299	0.77	-0.45	0.68	0.48	-0.61	2.25
5.235	6.023	-60.97	140.43	0.300	0.97	-0.60	1.12	0.61	-0.98	3.29
6.023	6.727	-60.89	140.54	0.318	2.44	-1.79	4.44	1.63	-3.76	11.29
6.727	7.537	-60.85	140.62	0.367	1.87	-1.23	2.71	1.16	-2.35	7.38
7.537	8.125	-60.78	140.73	0.376	1.73	-0.96	1.72	0.96	-1.58	5.33
8.125	9.105	-60.68	140.89	0.377	1.71	-0.87	1.36	0.87	-1.31	4.61
9.105	9.786	-60.56	141.09	0.378	1.93	-0.94	1.27	0.94	-1.27	4.70
9.786	11.056	-60.40	141.36	0.382	2.09	-1.07	1.65	1.02	-1.58	5.54
11.056	12.474	-60.18	141.72	0.409	3.13	-1.85	3.54	1.66	-3.16	10.28
12.474	13.739	-59.87	142.15	0.436	2.46	-1.24	1.36	1.16	-1.40	5.58
13.739	14.609	-59.53	142.58	0.441	5.83	-2.27	-0.02	1.87	-1.08	7.42
14.609	15.974	-59.42	142.84	0.441	3.35	-1.65	1.21	1.43	-1.42	6.41
15.974	17.235	-59.11	143.24	0.450	3.86	-1.90	1.37	1.66	-1.60	7.43
17.235	18.007	-58.95	143.44	0.485	9.39	-5.77	10.47	4.78	-8.99	29.61
18.007	18.636	-58.81	143.60	0.503	18.77	-12.58	27.17	10.25	-22.37	69.29
18.636	19.535	-58.33	144.04	0.482	10.40	-5.51	5.71	4.72	-5.59	22.92
19.535	20.765	-56.90	145.05	0.460	10.91	-4.80	-0.47	4.18	-1.23	13.62

Relative plate motion of South America respect to a fixed Nubia, as determined from the REDBACK noise-reduction software (Iaffaldano and DeMets, 2016). Angular velocities (ω) describe a counter-clockwise rotation as a forward motion (from older to younger age). Ages are assigned to each reversal according to the GTS20 magnetic anomaly timescale from Ogg (2020) (Table A.2).

Supplementary Table A.4: Upper triangle values of the symmetrical matrix operator **P**

Plate	c_{xx}	c_{xy}	c_{xz}	c_{yy}	c_{yz}	c_{zz}
AN[a]	23.773	-1.646	2.428	20.539	1.978	8.330
NA[a]	17.418	2.314	-0.801	15.951	4.708	8.894
NB[a]	75.804	-47.132	-51.938	139.690	-33.078	129.794
PA[a]	32.120	-13.764	-4.192	41.179	-5.014	41.696
SA[a]	8.975	5.444	3.523	12.925	-2.832	14.354
SA[b]	8.884	5.443	3.512	12.936	-2.800	14.279
SO[a]	4.284	-3.021	0.668	3.316	0.772	6.391

Operator **P** links a vectorial space of Euler-vector change experienced by a given plate ($\Delta\vec{\omega}$), to the torque variation responsible for the motion change ($\Delta\vec{M}$), as $\Delta\vec{M} = \mathbf{P}\ \Delta\vec{\omega}$. Viscosity of the upper mantle and asthenosphere are set to $1.5 \cdot 10^{21}$ and $5 \cdot 10^{19}$ Pa $\cdot$ s, respectively (e.g. Fjeldskaar, 1994; Mitrovica and Forte, 2004). Depth of the lithosphere-asthenosphere boundary is set to a global 180 km.

[a] Calculated using the spacial distribution of the plate at 7.0 Ma, based on the model of Matthews et al. (2016). Used for the torque variation at focus period 1 (see reference in main text).

[b] Same as in [a], but for a the geometry at 11.5 Ma, used for the torque variation at focus period 2.

Appendix B. Supplementary Figures

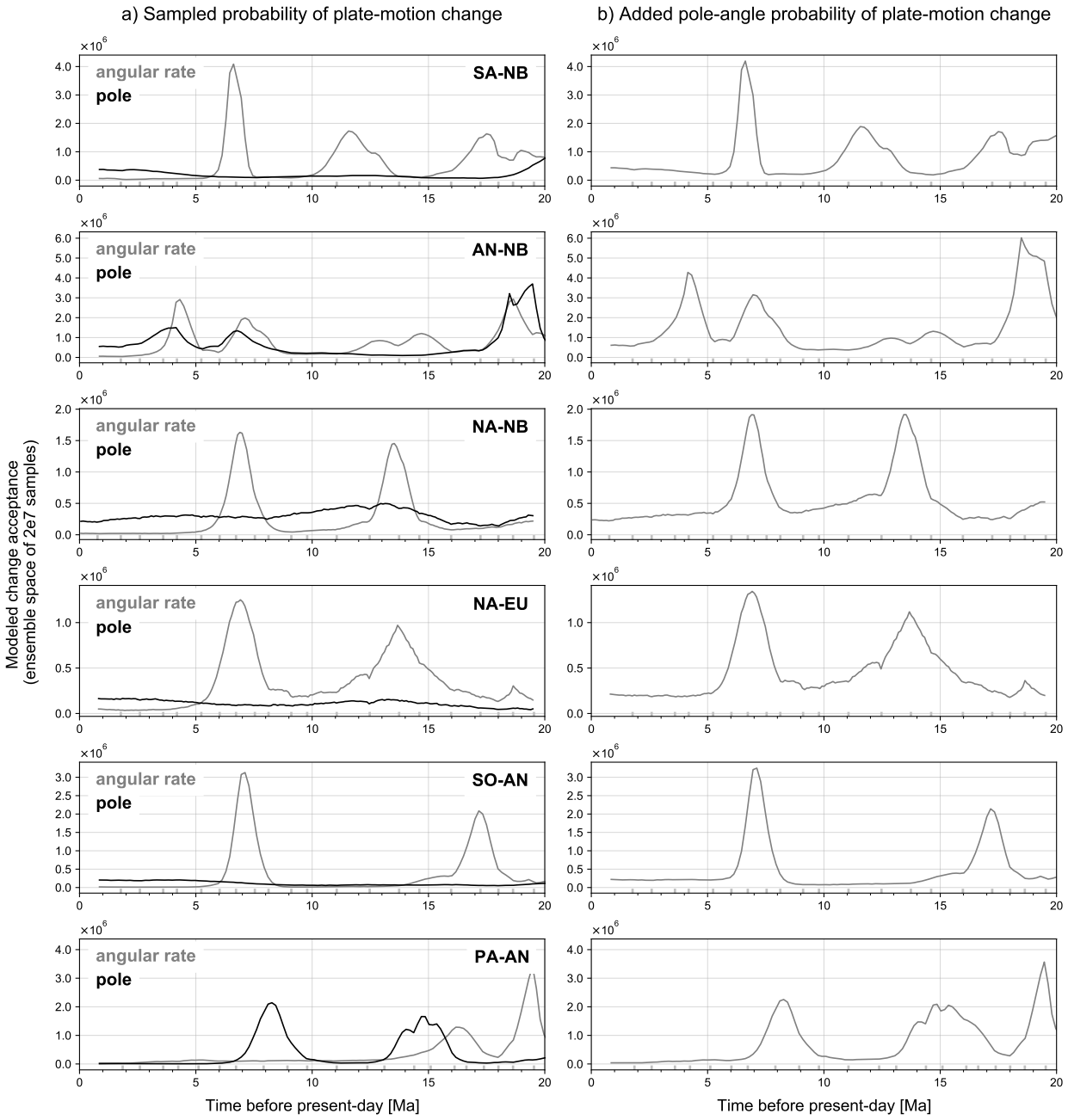

Supplementary Figure B.1: Sampled probability of plate-motion change for plates within the Atlantic region in the last 20 Myr. a) Gray solid curves report changes in angular velocity, black solid curves refer to changes in stage Euler poles. b) Gray curve plots the summation of plate-change probability for angular velocity and Euler Pole. Gray vertical ticks above the bottom axes mark the times for which finite rotations are available.

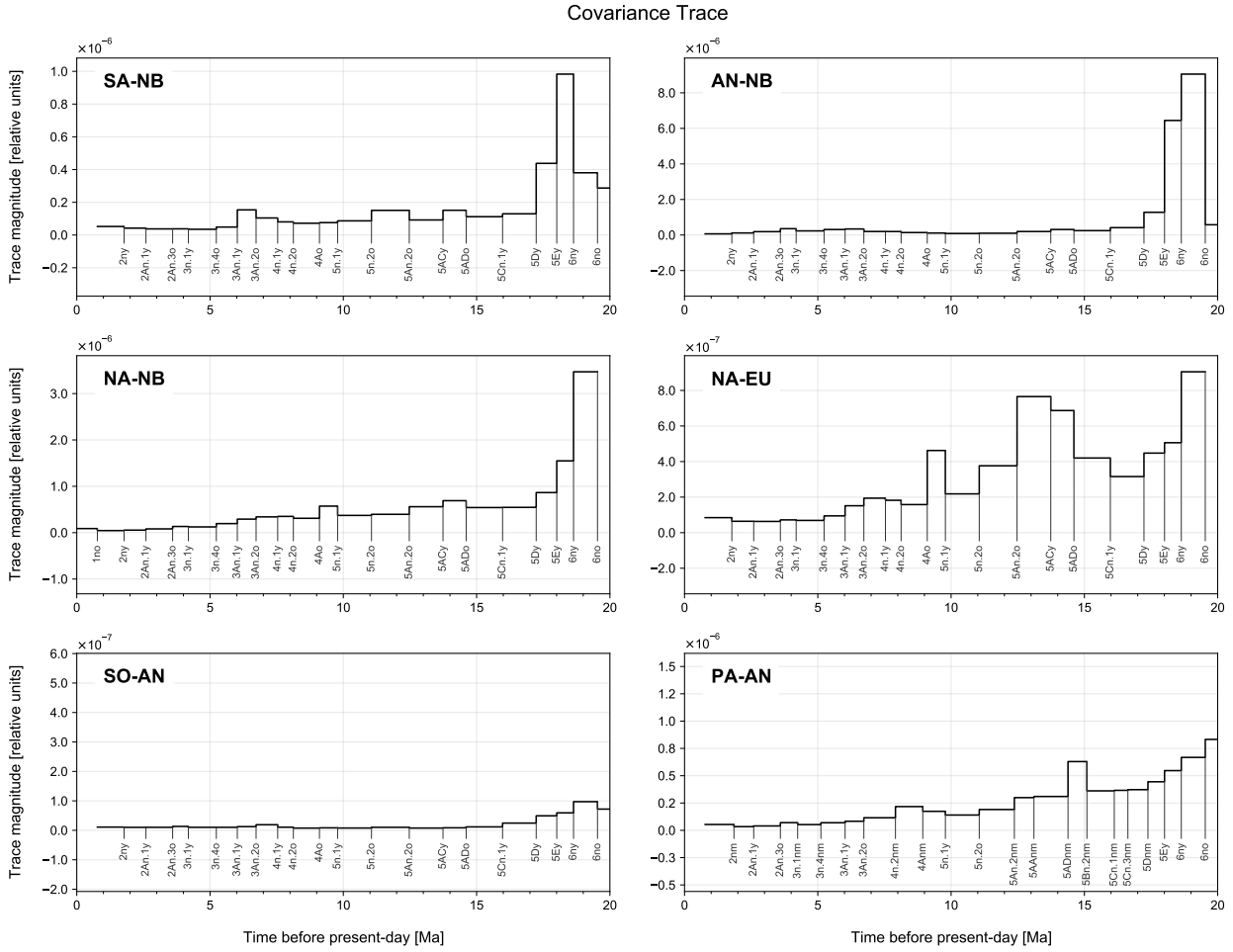

Supplementary Figure B.2: Trace of the covariance matrix for the Euler vector sequence of Nubia-South America (NB-SA), Nubia-Antarctica (NB-AN), Somalia-Antarctica (SO-AN), Nubia-North America (NB-NA), Eurasia-North America (EU-NA), and Pacific-Antarctica (PA-AN). Black solid curves show the variation in the trace for each corresponding Euler vector covariance matrix. Vertical lines and labels make reference to the corresponding magnetic reversal, as obtained from the GTS20 geomagnetic polarity time scale (Ogg, 2020, Table A.2).

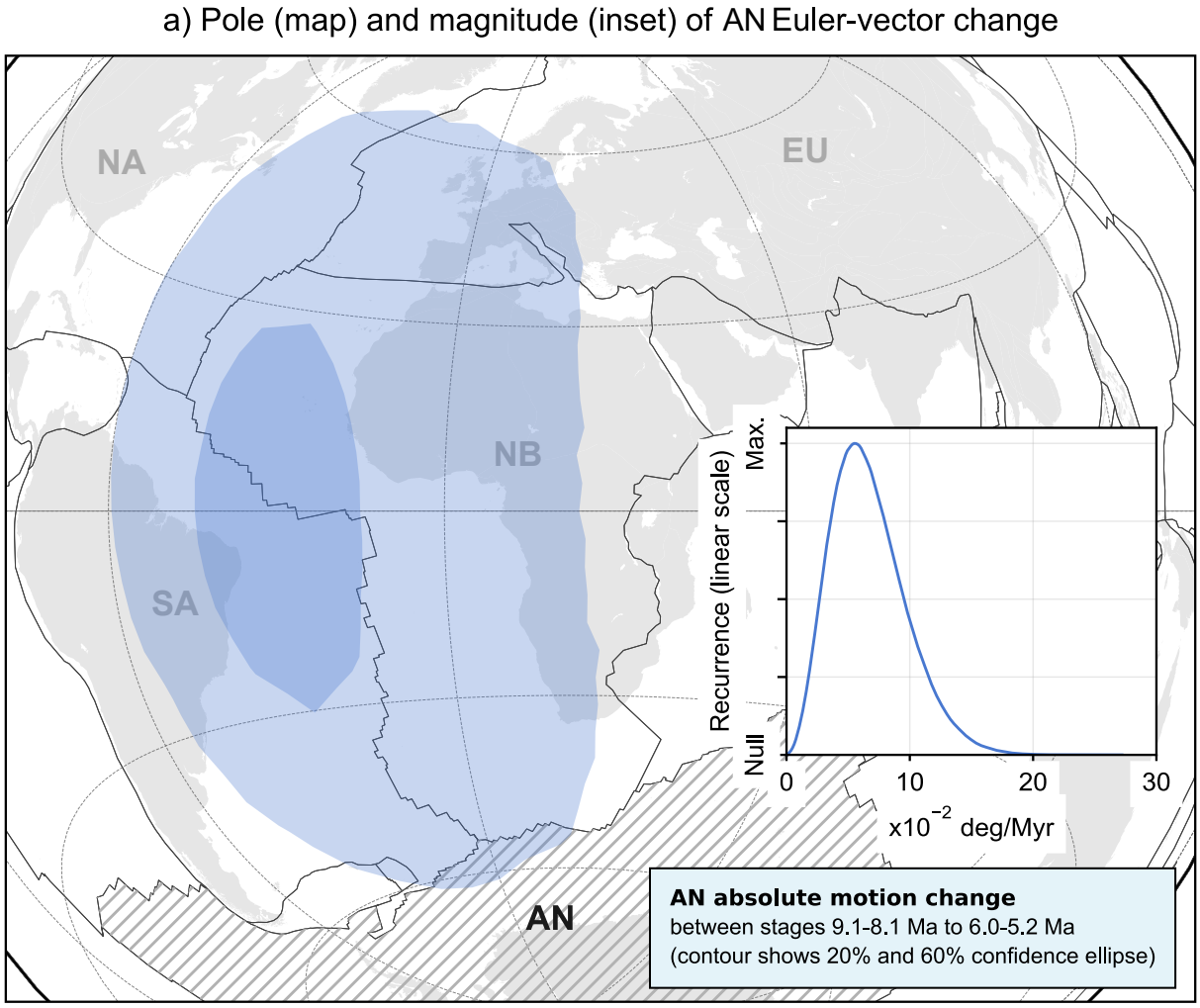

Supplementary Figure B.3: Antarctica absolute plate-motion change between stages 9.1 to 8.1 Ma (reversals 4Ao to 4n.2o) and 6.0 to 5.2 Ma (reversals 3An.1y to 3n.4o). Map shows the 20% and 60% confidence ellipses for the AN Euler pole change (dark and lighter blue, respectively), from and Euler vector ensemble of 10^6 samples. Inset shows the magnitude-change distribution for the aforementioned Euler-vector ensemble. Map uses Lambert Azimuthal Equal-Area projection centered at 0°N, 20°E.

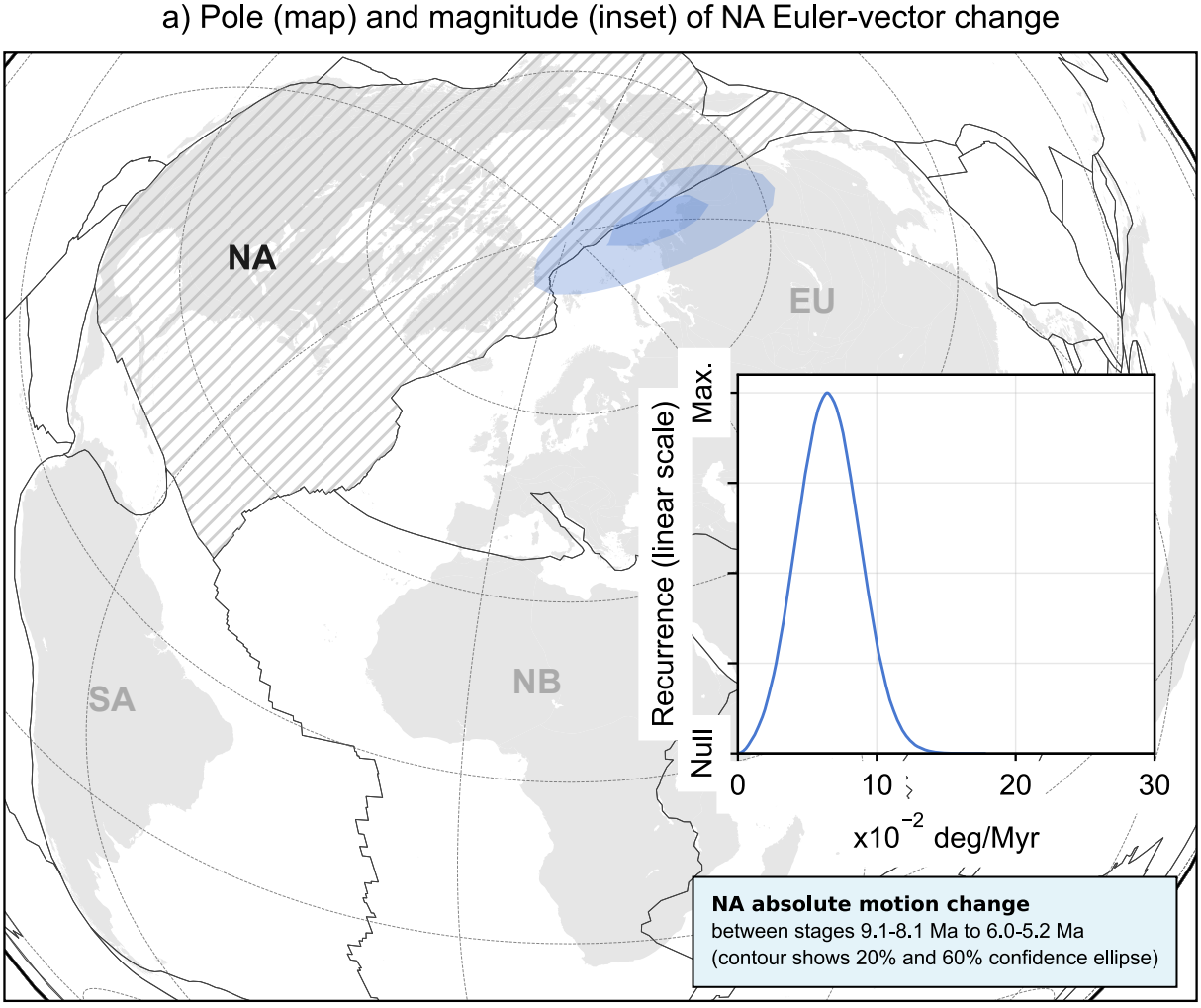

Supplementary Figure B.4: North-America absolute plate-motion change between stages 9.1 to 8.1 Ma (reversals 4Ao to 4n.2o) and 6.0 to 5.2 Ma (reversals 3An.1y to 3n.4o). Map shows the 20% and 60% confidence ellipses for the NA Euler pole change (dark and lighter blue, respectively), from and Euler vector ensemble of 10^6 samples. Inset shows the magnitude-change distribution for the aforementioned Euler-vector ensemble. Map uses Lambert Azimuthal Equal-Area projection centered at 45°N, 16°E.

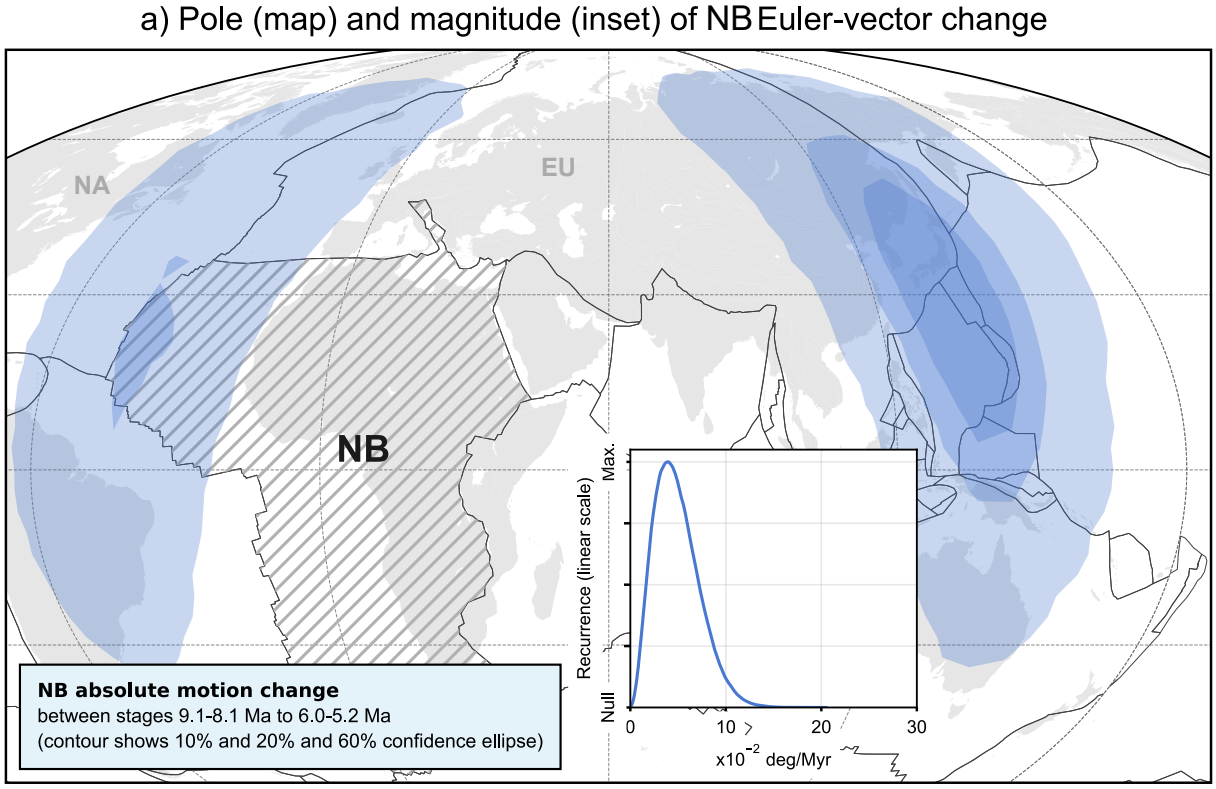

Supplementary Figure B.5: Nubia absolute plate-motion change between stages 9.1 to 8.1 Ma (reversals 4Ao to 4n.2o) and 6.0 to 5.2 Ma (reversals 3An.1y to 3n.4o). Map shows the 10%, 20% and 60% confidence ellipses for the NB Euler pole change (dark and lighter blue, respectively), from and Euler vector ensemble of 10^6 samples. Inset shows the magnitude-change distribution for the aforementioned Euler-vector ensemble. Map uses Mollweide projection centered at 60°E.

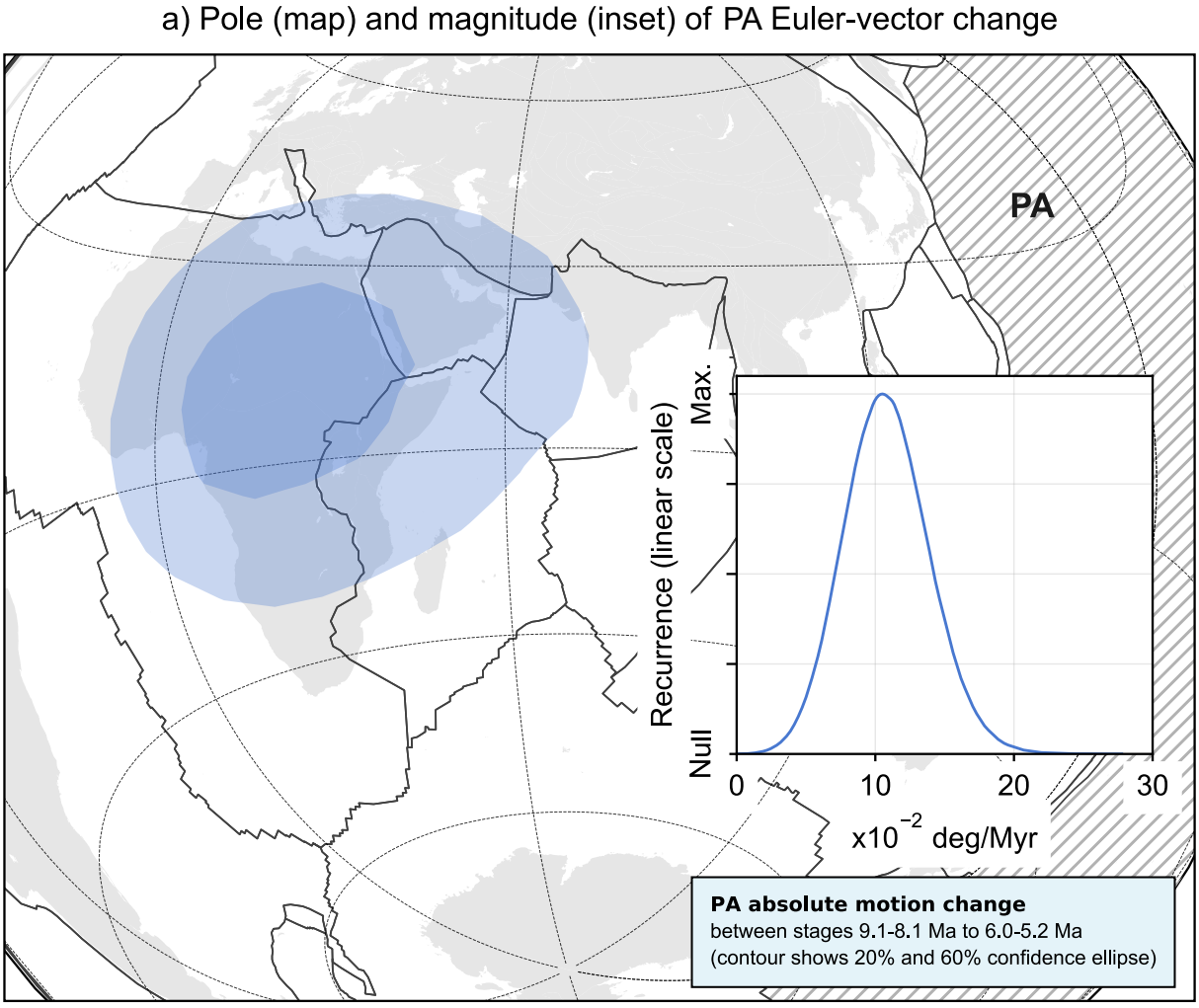

Supplementary Figure B.6: Pacific absolute plate-motion change between stages ∼9.8 to ∼9.1 Ma and ∼6.0 to ∼5.2 Ma. Map shows the 20% and 60% confidence ellipses for the PA Euler pole change (dark and lighter blue, respectively), from and Euler vector ensemble of 10^6 samples. Inset shows the magnitude-change distribution for the aforementioned Euler-vector ensemble. Map uses Lambert Azimuthal Equal-Area projection centered at -10°N, 70°E.

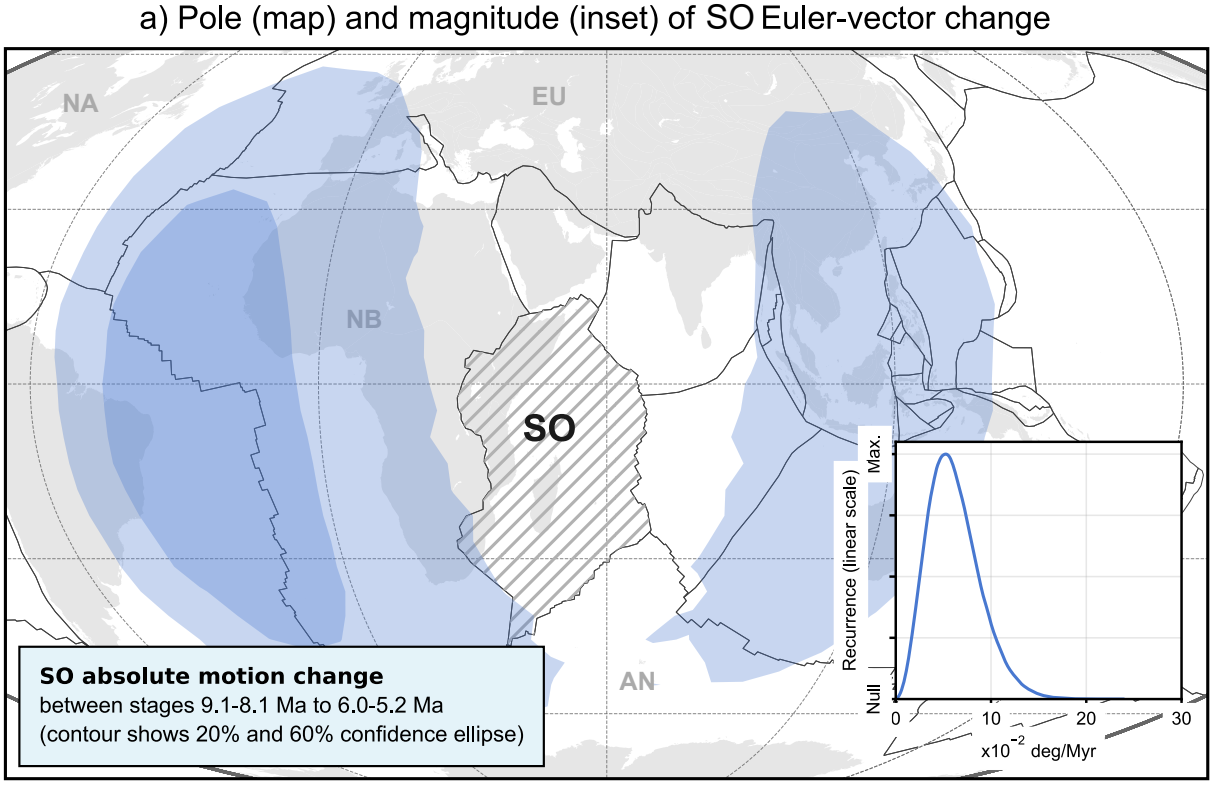

Supplementary Figure B.7: Somalia absolute plate-motion change between stages 9.1 to 8.1 Ma (reversals 4Ao to 4n.2o) and 6.0 to 5.2 Ma (reversals 3An.1y to 3n.4o). Map shows the 20% and 60% confidence ellipses for the NB Euler pole change (dark and lighter blue, respectively), from and Euler vector ensemble of 10^6 samples. Inset shows the magnitude-change distribution for the aforementioned Euler-vector ensemble. Map uses Mollweide projection centered at 60°E.

References

Croon, M.B., Cande, S.C., Stock, J.M., 2008. Revised pacific-antarctic plate motions and geophysics of the menard fracture zone. Geochemistry, Geophysics, Geosystems 9. doi:10.1029/2008GC002019.

DeMets, C., Iaffaldano, G., Merkouriev, S., 2015. High-resolution Neogene and Quaternary estimates of Nubia-Eurasia-North America Plate motion. Geophysical Journal International 203, 416–427. doi:10.1093/gji/ggv277.

DeMets, C., Merkouriev, S., 2019. High-resolution reconstructions of South America plate motion relative to Africa, Antarctica and North America: 34 Ma to present. Geophysical Journal International 217, 1821–1853. doi:10.1093/gji/ggz087.

DeMets, C., Merkouriev, S., Sauter, D., 2021. High resolution reconstructions of the Southwest Indian Ridge, 52 Ma to present: implications for the breakup and absolute motion of the Africa plate. Geophysical Journal International 226, 1461–1497.

Fjeldskaar, W., 1994. Viscosity and thickness of the asthenosphere detected from the Fennoscandian uplift. Earth and Planetary Science Letters 126, 399–410.

Iaffaldano, G., DeMets, C., 2016. Late Neogene changes in North America and Antarctica absolute plate motions inferred from the Mid-Atlantic and Southwest Indian Ridges spreading histories. Geophysical Research Letters 43, 8466–8472. doi:10.1002/2016GL070276.

Matthews, K.J., Maloney, K.T., Zahirovic, S., Williams, S.E., Seton, M., Müller, R.D., 2016. Global plate boundary evolution and kinematics since the late Paleozoic. Global and Planetary Change 146, 226–250. doi:10.1016/j.gloplacha.2016.10.002.

Mitrovica, J.X., Forte, A.M., 2004. A new inference of mantle viscosity based upon joint inversion of convection and glacial isostatic adjustment data. Earth and Planetary Science Letters 225, 177–189.

Ogg, J., 2020. Geomagnetic polarity time scale, in: Geologic time scale 2020. Elsevier, pp. 159–192.